Received: 23 August 2016 | Revised: 8 September 2017 | Accepted: 23 October 2017

DOI: 10.1002/asl.807

Atmospheric Science Letters RMetS

RESEARCH ARTICLE

Differences in the fractions of ice clouds between eastern and western parts of Eurasian continent using CALIPSO in January 2007

Akira Yamauchi[1] | Kazuaki Kawamoto[1] | Hajime Okamoto[2]

[1]Graduate School of Fisheries and Environmental Sciences, Nagasaki University, Nagasaki, Japan

[2]Research Institute for Applied Mechanics, Kyushu University, Fukuoka, Japan

Correspondence
A. Yamauchi, Graduate School of Fisheries and Environmental Sciences, Nagasaki University, Nagasaki, Japan.
Email: akira19890620@gmail.com

Funding information
Arctic Challenge for Sustainability (ArCS); JSPS KAKENHI, Grant/Award numbers: JP15K7762, JP17H06139, 25247078; Research Institute for Applied Mechanics, Kyushu University

We investigated the difference in the fraction of ice (water) cloud bins between eastern and western parts of Eurasia using Cloud-Aerosol Lidar and Infrared Pathfinder Satellite Observation (CALIPSO) data in January 2007. The fraction of ice cloud bins between −25 and 0 °C was clearly larger in eastern Eurasia than in western Eurasia. A significantly increased (about 20–30%) fraction of ice-containing clouds is observed in eastern Eurasia in the cloud top temperatures range from −30 to −15 °C. The difference in ice cloud bin fractions between eastern and western Eurasia was remarkable between −20 and −5 °C, being about 20% greater in eastern Eurasia. The fraction of ice cloud bins in the lower troposphere (below 3 km) was larger in eastern Eurasia than in western Eurasia. These results indicate that the ice formation process was more promoted in the lower troposphere in eastern Eurasia than in western Eurasia. This is the first time such results have been obtained from cloud internal structure observations using the CALIPSO active sensor.

KEYWORDS
cloud physics, ice cloud, satellite observation

1 | INTRODUCTION

Clouds have a large impact on the hydrological system and Earth's energy budget. Many previous studies identified clouds as an important source of uncertainty when attempting to understand and predict global climate change (e.g., Dufresne & Bony, 2008; Stephens, 2005). Cloud effects are strongly regulated by their microphysical (particle size, number concentration, and mass density of water or ice particulates) and macrophysical (temporal frequency, height, geometrical thickness, and rainfall intensity) structures. For example, Kawamoto and Hayasaka (2008) reported that the surface radiative flux was dominated by cloud optical thickness and cloud cover. However, the details of the formation and growth processes of ice clouds remain unknown.

The formation and growth processes of ice clouds are very complicated compared with those of water clouds, and are not yet fully understood (Lohmann & Feichter, 2005) because the formation and growth processes of ice particles vary. Ice particle formation involves both homogeneous and heterogeneous freezing (contact freezing, immersion freezing, condensation nucleation, and deposition nucleation). At temperatures below −38 °C, ice particles are formed by homogeneous and heterogeneous freezing. In contrast, at temperatures above −38 °C, ice particles are formed entirely by heterogeneous freezing (Hoose & Möhler, 2012). Ladino Moreno, Stetzer, and Lohmann (2013) reported that contact freezing occurs at higher temperatures than immersion freezing. More ice-containing clouds are typically observed, with cloud top temperatures (CTT) from −20 to −10 °C, in dusty air conditions than in dust-free air conditions (Seifert *et al.,* 2010; Zhang *et al.,* 2012). The ice particle growth process has vapor growth, riming, and aggregation stages. At temperatures below −20 °C, the ice effective radius correlates with temperature, and the ice

effective radius increases with increasing temperature (Ou & Liou, 1995). Moreover, the ice effective radius increases with increasing cloud optical thickness (Takahashi, Hayasaka, & Okamoto, 2016). The shape of ice crystals depends on temperature and supersaturated water vapor density (Kobayashi, 1961).

In this study, we focused on the ice particle formation at temperatures greater than −40 °C. In addition, mixed-phase clouds are considered as ice clouds in this study. We considered only the bins for which CALIOP could successfully determine the phase classification, and compared two regions (eastern and western Eurasia) in January 2007. We chose January 2007 as a representative of the winter season.

This paper is arranged as follows. Section 2 describes the satellite and reanalysis data sets used in this study. Section 3 presents the main outcomes of this study, and shows the differences in the fractions of ice cloud bins between eastern and western parts of Eurasia. Finally, Section 4 discusses and summarizes the obtained results.

2 | DATA

2.1 | Satellite observations

We used Cloud-Aerosol Lidar and Infrared Pathfinder Satellite Observation (CALIPSO) satellite data for the period of January 2007. CALIPSO is also part of the satellite constellation of passive and active sensors called the A-Train (including OCO-2, GCOM-W1, Aqua, CALIPSO, CloudSat, and Aura) (Stephens *et al.,* 2002). A-train satellites cross the equator within a few minutes of one another at around 1:30 p.m. (13:30) local time from a 705 km altitude orbit. CALIPSO was launched in April 2006, and carries a Cloud-Aerosol Lidar with Orthogonal Polarization (CALIOP) (Winker, Hunt, & McGill, 2007). The CALIOP can measure the backscattering coefficient at 532 nm (its horizontal and vertical resolutions are 0.33 km × 30 m below 8.2 km and 1.0 km × 60 m above 8.2 km, respectively) and 1064 nm (its horizontal and vertical resolutions are 0.33 km × 60 m below 8.2 km and 1.0 km × 60 m above 8.2 km, respectively) and the depolarization ratio is retrieved at 532 nm. We used CALIPSO level 1B product version 3. We sampled 418 orbits (83 vertical bins × approximately 37 081 profiles per orbit) during the study period. Each 3° × 3° latitude–longitude grid box was sampled by about 7 orbits in the tropics, by about 10 orbits in the mid latitude, and by about 37 orbits in the high latitudes. In this study, we used part of the Kyushu University (KU) products (Hagihara, Okamoto, & Yoshida, 2010; Okamoto, Sato, & Hagihara, 2010; Sato & Okamoto, 2011; Yoshida, Okamoto, Hagihara, & Ishimoto, 2010). Yoshida *et al*. (2010) developed a method to discriminate cloud particle types (KU-type) using the CALIOP backscattering coefficient and depolarization ratio. The cloud region of this product was determined from a KU-mask (Hagihara *et al.,* 2010) using only CALIOP data with a 240 m horizontal resolution. One pixel of KU-type product has 83 vertical bins (vertical resolution is 240 m), and 1 orbit has approximately 37081 pixels. Cloud particle phase discrimination is performed for each bin. The cloud particles were classified into six types: warm water, supercooled water, horizontally oriented plates (2D-plate), randomly oriented ice crystals (3D-ice), unknown1 (mixture of 2D-plate and 3D-ice), and unknown2 (water or 3D-ice). In this study, we used the KU dataset and defined an "ice cloud" as a 2D-plate, 3D-ice, and unknown1. Furthermore, we defined "water cloud" as warm water and supercooled water. The unknown2 bins were excluded from our analyses to avoid ambiguity. The fraction of unknow2 in each cloud bin temperature is less than 0.1%, and we do not have any significant changes even if we ignore unknown2. This classification of the cloud particle type was conducted using CALIOP data, and the CloudSat product used in this study contained only altitude and temperature profiles from the European Center for Medium-Range Weather Forecasts (ECMWF-AUX) (Partain, 2007). In this study, the fractions of ice-containing clouds ($F_{ice\_con.}$) and water clouds (F_{water}), and the fractions of ice cloud bins (F_{ice_bin}) and water cloud bins (F_{water_bin}) are defined as:

$$F_{ice\_con.} = N_{ice\_con.}/(N_{ice\_con.} + N_{water}) \quad (1)$$

$$F_{water} = N_{water}/(N_{ice\_con.} + N_{water}) \quad (2)$$

$$F_{ice\_bin} = N_{ice\_bin}/(N_{ice\_bin} + N_{water\_bin}) \quad (3)$$

$$F_{water\_bin} = N_{water\_bin}/(N_{ice\_bin} + N_{water\_bin}) \quad (4)$$

where $N_{ice\_con.}$ and N_{water} are numbers of ice-containing clouds and water clouds, and N_{ice_bin} and N_{water_bin} are the numbers of the ice and water bins, respectively, that CALIOP could successfully detect among the entire cloud bins. We analyzed only the cloud bins whose CTT were warmer than −40 °C. We defined "cloud" as the bins from the highest one to the lowest one that the lidar could penetrate and recognize as cloudy bin using KU-mask, and $N_{ice\_con.}$ was defined as containing ice phase bin in the cloud. In the case of optically thick ice cloud, we sampled the cloud bins for which the CALIOP lidar signal was not attenuated from cloud top, and it could observe cloud optical thickness up to about 7 (H. Okamoto, personal communication, 2017).

2.2 | Reanalysis data

We used the temperature 2 m above ground, surface downward long-wave radiation flux, and surface upward long-wave radiation flux from the Japanese 55-year reanalysis (JRA-55) data. This is based a spatial and temporal

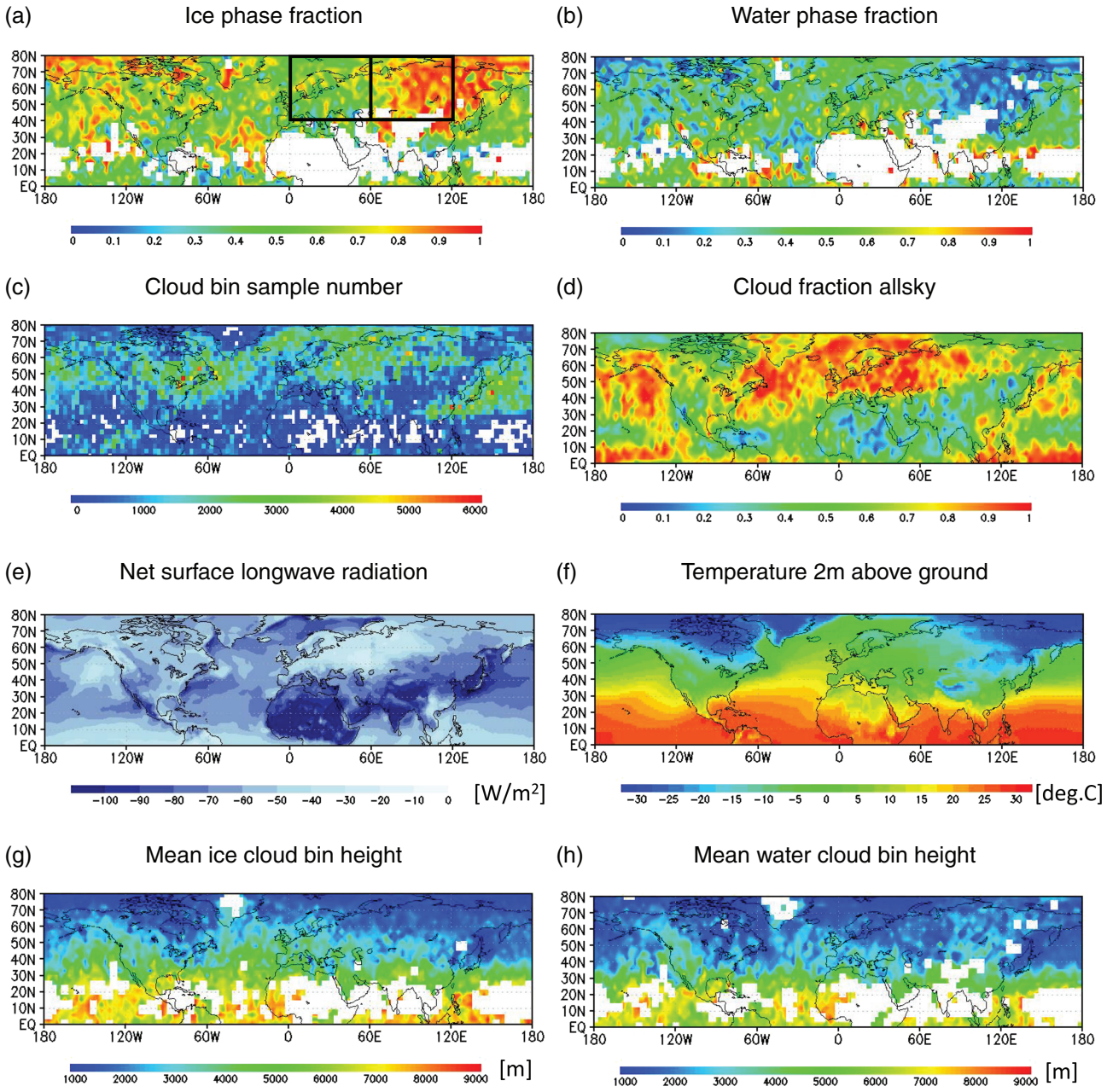

FIGURE 1 Northern Hemisphere distribution in January 2007 of: (a) fraction of ice cloud bins between −25 and 0 °C, (b) fraction of water cloud bins between −25 and 0 °C, (c) the total sample numbers of (a) and (b), (d) fraction of clouds in the whole sky, (e) net surface long-wave radiation, (f) temperature 2 m above ground, and (g) the mean height of ice cloud bins with temperatures of 0 to −25 °C, (h) same as (g) but for water cloud bins. (a)–(d), (g), and (h) are from CALIPSO data, with a resolution of 3.0° latitude by 3.0° longitude. (e), (f) are from JRA-55 data, with a resolution of 1.25° latitude by 1.25° longitude

resolution of 1.25° × 1.25°, 37 vertical levels, 6-hourly measurements, and four-dimensional variational data assimilation (Harada *et al.,* 2016; Kobayashi *et al.,* 2015). JRA-55 was released by the Japan Meteorological Agency in 2014, and has a longer analysis period than the previous Japanese reanalysis product (JRA-25) (Onogi *et al*., 2007). It covers a long period from 1958. In this study, the surface net long-wave radiation flux (SLR_{net}) was defined as:

$$SLR_{net} = L_{\downarrow} - L_{\uparrow} \quad (5)$$

where $L_{\downarrow}$ is the surface downward long-wave radiation flux and $L_{\uparrow}$ is the surface upward long-wave radiation flux.

3 | RESULTS

3.1 | Northern Hemisphere maps

The fraction of ice cloud bins between −25 and −0 °C was about 20% higher in eastern Eurasia than in western Eurasia. Figure 1a and b show the fractions of ice cloud bins (F_{ice_bin}, shown in Equation (3)) and water cloud bins (F_{water_bin}, shown in Equation (4)) in each 3° × 3° latitude–longitude box between −25 and 0 °C using the KU-type and ECMWF-AUX products, and Figure 1c shows the total sample numbers of Figure 1a and b. N_{ice_bin} and N_{water_bin} are the numbers of ice and water bins in the atmospheric

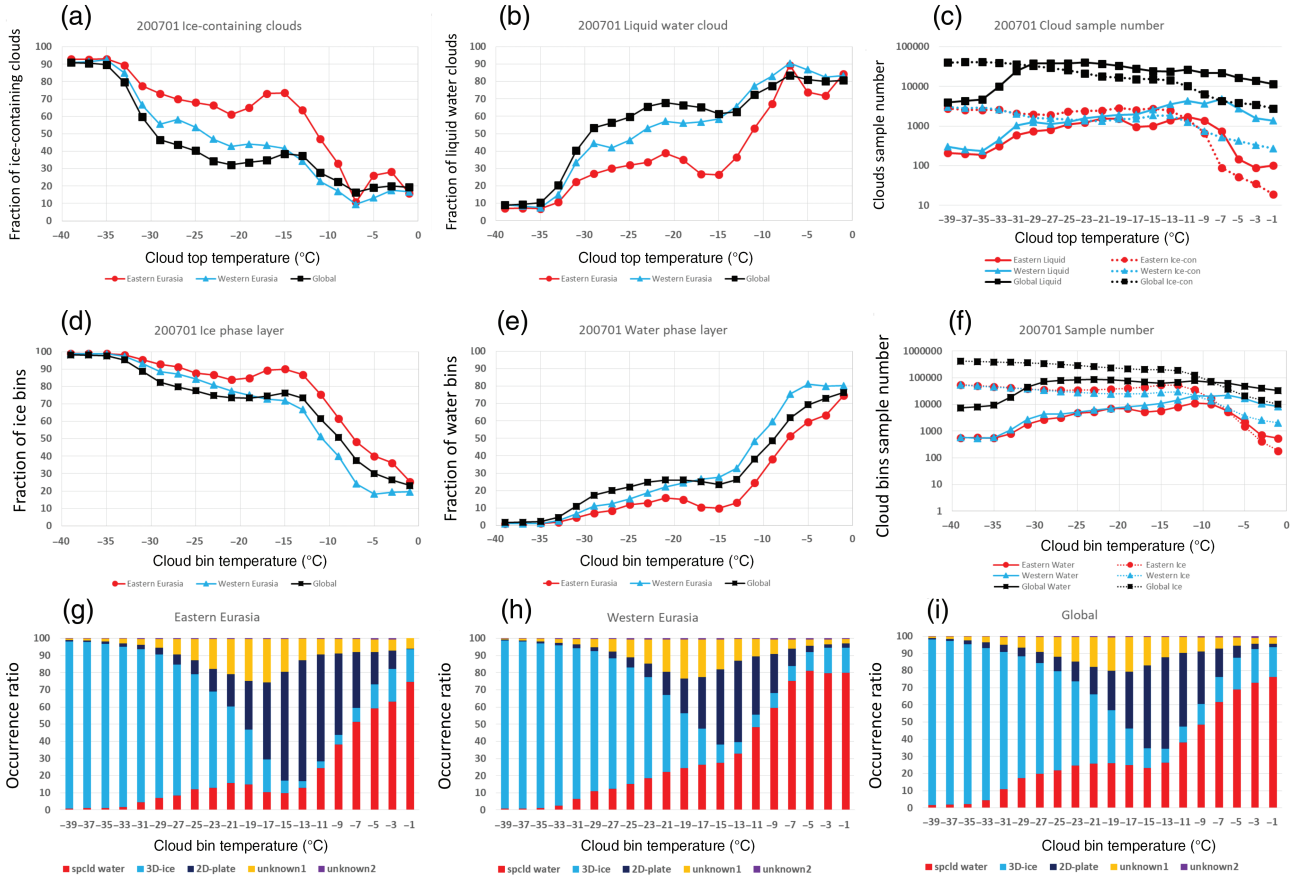

FIGURE 2 Fractions of (a) ice-containing clouds and (b) water clouds as function as a cloud top temperature (at 2 °C intervals), the red line represents eastern Eurasia (40°–80°N, 60°–120°E), the blue line represents western Eurasia (40°–80°N, 0°–60°E), and the black line represents the global value (90°S–90°N, 180°W–180°E, (c) the sample numbers of ice-containing (solid) and water (dotted) clouds in eastern Eurasia (red), western Eurasia (blue), and globe (black). Fractions of (d) ice bins and (e) water bins as a function of cloud bin temperature (at 2 °C intervals), (f) the sample numbers of ice and water bins in eastern Eurasia, western Eurasia, and globe. Properties of the occurrence ratios of each particle type in (g) eastern Eurasia, (h) western Eurasia, and (i) global value as a function of cloud bin temperature with intervals of 2 °C

column in Figure 1. The fractions of ice and water cloud bins over the Eurasian continent were very different between east of 60°E and west of 60°E. The fraction of ice bins was higher in eastern Eurasia than in western Eurasia, whereas the fraction of water cloud bins was lower in eastern Eurasia. These results suggest that the formation of ice clouds occurred more readily in eastern Eurasia than in western Eurasia. Figure 1d shows the cloud fractions in each 3° × 3° latitude–longitude box from the KU-mask. The cloud fraction is the rate of pixels covered by clouds when the CloudSat and CALIPSO satellites passed over. The cloud fraction was lower in eastern Eurasia than in western Eurasia. Figure 1e shows the surface net long-wave radiation flux (SLR_{net}, shown in Equation (5)) from JRA-55. The SLR_{net} was lower in eastern Eurasia than in western Eurasia, with strong radiative cooling caused by the low cloud fraction in eastern Eurasia. Figure 1f shows the temperature 2 m above ground from JRA-55. This temperature was lower in eastern Eurasia where radiative cooling was strong. Figure 1g shows the mean height of ice cloud bins when cloud temperatures are −25 to 0 °C. Figure 1h shows the same as Figure 1g, but for water cloud bins. The mean height of water cloud bins in eastern Eurasia was higher than in western Eurasia, and the mean height of ice cloud bins in eastern Eurasia was lower than in western Eurasia. Consequently, the clouds over eastern Eurasia might be influenced by the ground surface, and we consider that this could be one of the reasons for the larger fraction of ice clouds in the region.

In the next section, we discuss how large the fraction of ice cloud bins was in eastern Eurasia in each temperature range.

3.2 | Comparison of the fractions of ice-containing clouds and ice cloud bins in each CTT and cloud bin temperature range

A significantly increased fraction of ice-containing clouds is observed in eastern Eurasia in the CTT range from −30 to −15 °C. Figure 2a and b shows the relationship between the fraction of ice-containing (water) clouds (shown in Equations (1) and (2)) and CTT. CTT from ECMWF-AUX is binned in 2 °C intervals between −40 and 0 °C. The presentation of the data in Figure 2a and b is best comparable with the existing studies of Seifert *et al.* (2010), Kanitz *et al.* (2011) and Zhang, Wang, and Liu (2010); Zhang

et al. (2012). Figure 2a shows the fraction of ice-containing clouds as a function of CTT in eastern Eurasia (40°–80°N, 60°–120°E), western Eurasia (40°–80°N, 0°–60°E), and globe (land only). Figure 2b shows the same as Figure 2a, but for water clouds. Figure 2c shows the sample numbers of ice-containing (solid) and water (dotted) clouds in eastern Eurasia, western Eurasia, and globe. The fraction of ice-containing clouds increases as CTT decreases. However, the fractions of ice-containing clouds in eastern and western Eurasia in each CTT behaved differently, and the fraction of ice-containing (water) clouds in eastern Eurasia was higher (lower) than in western Eurasia and globe with peak difference about 30% around −15 °C. At CTT around −15 °C, where ice-containing clouds dominate, these results suggest that the ice nucleus may work effectively in ice-containing clouds in eastern Eurasia.

The fractions of ice and water cloud bins were very different at temperatures higher than −20 °C. Figure 2d and e show the relationship between the fraction of ice (water) cloud bins (shown in Equations (3) and (4)) and cloud bin temperature. N_{ice_bin} and N_{water_bin} are the numbers of the ice and water bins as a function of cloud bin temperature. Cloud temperature from ECMWF-AUX is binned in 2 °C intervals between −40 and 0 °C. Figure 2d shows the fraction of ice cloud bins as a function of cloud bin temperature in eastern Eurasia, western Eurasia, and globe. Figure 2e shows the same as Figure 2d, but for water cloud bins. Figure 2f shows the sample numbers of ice (solid) and water (dotted) cloud bins in eastern Eurasia, western Eurasia, and globe. Here, we are not convinced that of much can be concluded about the range between −5 and 0 °C, accounting for the much smaller number of samples in eastern Eurasia. The fraction of ice cloud bins sharply increases from −15 to −5 °C (Figure 2d). A significantly higher fraction of ice cloud bins was observed in eastern Eurasia in the temperature range from −20 to −5 °C, and a lower fraction of water cloud bins was observed in this temperature range (Figure 2e). Compared with the global and western Eurasian levels, the fraction of ice cloud bins in eastern Eurasia was about 20% larger between −20 and −5 °C, and the fraction of water cloud bins was about 20% lower. The temperature for fifty-fifty chance of ice and water changes between the two regions (eastern and western Eurasia) and globe: the global temperature for equal probability is about −10 °C, while it is closer to −8 °C for eastern Eurasia and −12 °C for western Eurasia. This would suggest that ice formation is more effective indeed in eastern than western Eurasia. At the temperatures higher than −20 °C, ice formation is mainly due to the immersion and contact freezing processes (Hoose & Möhler, 2012), indicating that these freezing processes were promoted to a larger extent in eastern Eurasia than both globe and in western Eurasia.

Figure 2g–i shows properties of the occurrence ratios of each particle type in (g) eastern Eurasia, (h) western Eurasia, and (i) global value as a function of cloud bin temperature with intervals of 2 °C. At the temperatures below −30 °C, most particles existed as 3D-plate. The 2D-plate occurrence ratio exhibited its maximum between −16 and −10 °C. The ratio of 2D-plate occurrence on eastern Eurasia between −5 and −20 °C was larger than those on western Eurasia and the globe. Those results showed that the increase in the fraction of ice cloud bins in eastern Eurasia was due to an increase in the 2D-plate particle type.

3.3 | Comparison of the fractions of ice and water cloud bins in each altitude

The extent of the difference in the fraction of ice cloud bins between eastern and western Eurasia was larger in the lower layer of the troposphere. Figure 3a and b show the relationship between the fraction of ice (water) cloud bins (shown in Equations (3) and (4)) and altitude. N_{ice_bin} and N_{water_bin} are the numbers of the ice and water bins as a function of altitude. Cloud temperature from ECMWF-AUX is binned in 500 m intervals between 0 and 8000 m. Figure 3a shows the fraction of ice cloud bins as a function of altitude in eastern Eurasia, western Eurasia, and globe. Figure 3b shows the same as Figure 3a but for water cloud bins. Figure 3c shows the sample numbers of ice (solid) and water (dotted) cloud bins in eastern Eurasia, western Eurasia, and the globe. Almost all of the clouds above 4 km were present as ice clouds. However, the fractions of ice and water cloud bins below 3 km in eastern and western parts of Eurasia were significantly different. The fraction of water cloud bins below 3 km was lower in eastern Eurasia than in western Eurasia, while the fraction of ice cloud bins was higher. The difference in the fraction of ice (water) cloud bins between eastern and western Eurasia displays a peak at around 1 km, and the fraction was about 40% higher (lower) in eastern Eurasia than in western Eurasia. These differences depend on the difference in cloud bin temperature at each altitude. Figure 3d shows the mean cloud bin temperature at each altitude. The mean cloud bin temperature around 1 km in eastern Eurasia was −13.6 °C, and in western Eurasia was −8.8 °C. We showed that the fraction of ice cloud bins sharply increased from −15 to −5 °C in Figure 2d, and cloud bin temperature around 1 km in eastern Eurasia reached around −15 °C, then the fraction of ice cloud bins did not greatly change in this temperature range. On the other hand, cloud bin temperature around 1 km in western Eurasia was warmer than in eastern Eurasia, and the fraction of ice cloud bins greatly changed in this temperature range. Those indicate that the immersion and contact freezing processes in eastern Eurasia were promoted in the lower layer.

4 | DISCUSSION AND CONCLUSIONS

We found that the fraction of ice cloud bins between −25 and 0 °C was larger in eastern than in western Eurasia in

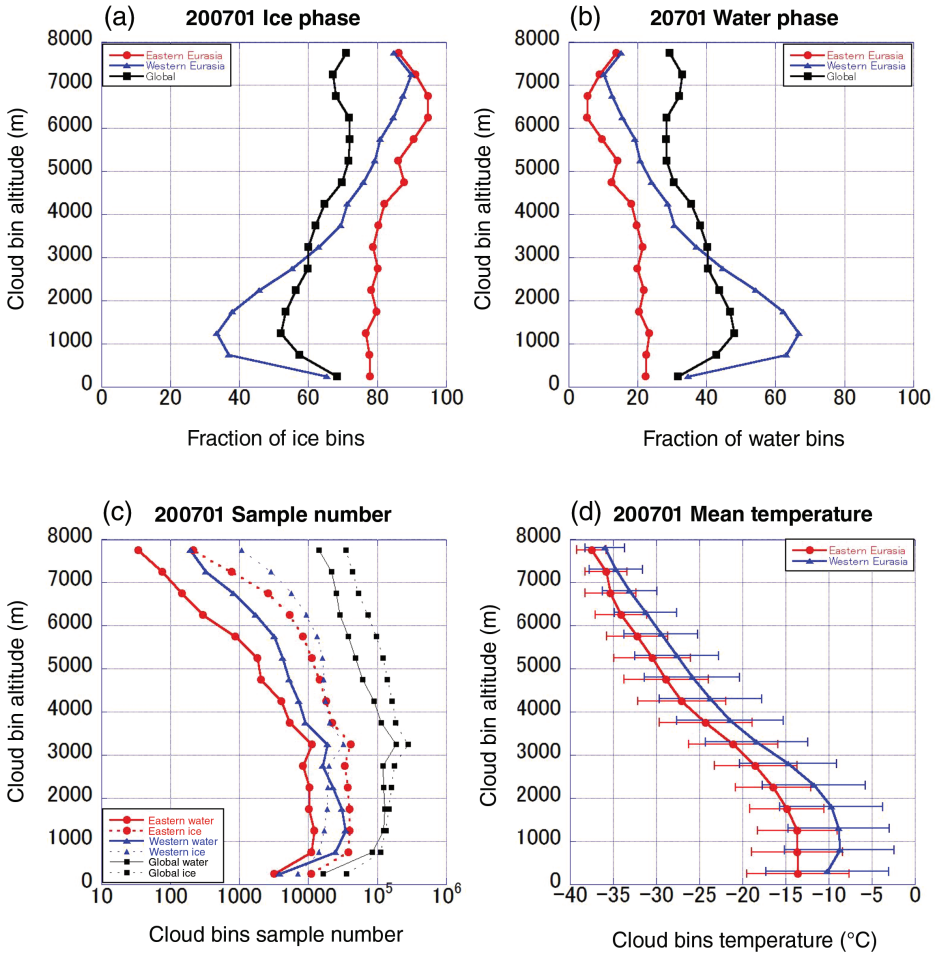

FIGURE 3 Fractions of (a) ice cloud bins and (b) water cloud bins as a function of cloud bin altitude (at 500 m intervals), the red line represents eastern Eurasia, the blue line represents western Eurasia, and the black line represents the global value, (c) the sample numbers of ice (solid) and water (dotted) cloud bins in eastern Eurasia (red), western Eurasia (blue), and globe (black), (d) mean cloud bin temperature as a function of cloud bin altitude, the red line represents eastern Eurasia, the blue line represents western Eurasia

January 2007. Eastern Eurasia had a lower cloud fraction than western Eurasia, which resulted in strong radiative cooling. The atmospheric temperature decreased due to radiative cooling from the ground surface. Therefore, the freezing layer is close to the ground surface in this region. We considered that the freezing layer was strongly affected by ice nuclei from the ground surface, caused by the changing altitude of the freezing layer, and thus the fraction of ice clouds increased. This indicates that the process of ice particle formation might be changed under the influence of atmospheric conditions.

The fraction of ice-containing clouds in eastern Eurasia was higher than in western Eurasia and globe with a peak difference of about 30% around −15 °C. The fraction of ice cloud bins between −20 and −5 °C was about 20% higher in eastern Eurasia than in western Eurasia. In this temperature range, ice particles are formed by the contact freezing and immersion freezing processes, and our results indicate that these formation processes were promoted in eastern Eurasia. Several previous observational studies examined that the change of the fraction of ice clouds as a function of CTT (e.g., Kanitz *et al.,* 2011; Seifert *et al.,* 2010; Zhang *et al.,* 2010, 2012). In this study, we focused on internal cloud change using cloud bin temperature and satellite active sensor. Hogan, Behera, O'Connor, and Illingworth (2004) showed the fraction of supercooled water for each temperature using Lidar In-Space Technology Experiment (LITE), and pointed out that the fraction of supercooled water decreased with falling temperature. A similar tendency was found in our result. However, our result suggests that the fraction of supercooled water at temperature above −10 °C shown in Hogan *et al.* (2004) is underestimated. Moreover, our study showed a large regional contrast between eastern and western Eurasia in the fraction of supercooled water bins. Cantrell and Heymsfield (2005) discussed the riming-splintering mechanism increasing the concentration of ice particles at temperature from about −10 to −5 °C, but we did not observe the sharp increase in fraction of ice bins at this temperature range. Therefore, we assume that the influence of this mechanism on clouds observed in this study was small.

Forest fires often occur around Siberia, and the soot particles spread out over eastern Eurasia (Damoah *et al.,* 2004). Atkinson *et al.* (2013) showed that feldspar is important as ice particle nuclei below −15 °C, and also reported that there are major sources of feldspar in Asia and Africa. We propose that these ice nuclei have an influence on the larger fraction of ice clouds in eastern Eurasia than in western Eurasia.

The fractions of ice and water cloud bins in the lower troposphere (below 3 km) were significantly different between eastern and western parts of Eurasia. The fraction of ice cloud bins below 3 km was higher in eastern Eurasia than in western Eurasia. This suggests that the formation of

ice particles in eastern Eurasia is initiated at a lower altitude, closer to the ground surface, than in western Eurasia. We also considered that the impact of the ground surface on ice particle nuclei was larger in eastern Eurasia than in western Eurasia. The supersaturation and dynamics are important factors for ice particle formation and the subsequent evolution of the ice phase in the cloud layer (Korolev, 2007; Korolev & Field, 2008; Morrison *et al.,* 2012); however, these parameters cannot be measured from CALIPSO. A future challenge will be to investigate the influence of those parameters using numerical models. Furthermore, Yoshida *et al*. (2010) discussed the difference in the fraction of cloud phase between KU-type and Vertical Feature Mask (VFM) cloud phase product, and pointed out the possibility that the VFM product tended to misclassify 2D-plate and 3D-ice as water. Moreover, Radar and Lidar (DARDAR) products (Delanoë & Hogan, 2008, 2010) can perform cloud particle phase discrimination for each bin similar to KU products. We will perform a comparative study of KU products with DARDAR products in future work. The difference in the fraction of ice and water between eastern and western Eurasia was similarly obtained in January 2008 (not shown). However, the platform tilting angle was changed to 3.0° in January 2008, and the 2D-plate could hardly be observed, and these results showed that the backscattering characteristics of the 2D-plate substantially changed by modifying the platform tilting angle. Those results showed that 2D-plate could be misclassified to 3D-ice or unknown1 after November 2007. For future work, we plan to develop an algorithm that corresponds to the platform tilting angle of 3.0°.

The radiative properties change according to ice cloud altitude and ice water content (Liou, 1986). We consider that the radiative properties differed between eastern and western parts of Eurasia due to the difference in the fraction of ice clouds in the lower troposphere. In future studies, we will investigate the difference in radiative properties between eastern and western parts of Eurasia.

ACKNOWLEDGEMENTS

The CloudSat data products were provided by the CloudSat Data Processing Center at the Cooperative Institute for Research in the Atmosphere, Colorado State University. This work was supported in part by the Collaborative Research Program of the Research Institute for Applied Mechanics, Kyushu University. H.O. is supported by JSPS KAKENHI grant numbers 25247078, JP17H06139, JP15K7762, and the Arctic Challenge for Sustainability (ArCS) project.

REFERENCES

Atkinson, J. D., Murray, B. J., Woodhouse, M. T., Whale, T. F., Baustian, K. J., Carslaw, K. S., … Malkin, T. L. (2013). The importance of feldspar for ice nucleation by mineral dust in mixed-phase clouds. *Nature*, *498*, 355–358. https://doi.org/10.1038/nature12278

Cantrell, W., & Heymsfield, A. (2005). Production of ice in tropospheric clouds: A review. *Bulletin of the American Meteorological Society*, *86*, 795–807. https://doi.org/10.1175/BAMS-86-6-795

Damoah, R., Spichtinger, N., Forster, C., James, P., Mattis, I., Wandinger, U., … Stohl, A. (2004). Around the world in 17 days – hemispheric-scale transport of forest fire smoke from Russia in May 2003. *Atmospheric Chemistry and Physics*, *4*, 1311–1321.

Delanoë, J., & Hogan, R. J. (2008). A variational scheme for retrieving ice cloud properties from combined radar, lidar, and infrared radiometer. *Journal of Geophysical Research*, *113*, D07204. https://doi.org/10.1029/2007JD009000

Delanoë, J., & Hogan, R. J. (2010). Combined CloudSat-CALIPSO-MODIS retrievals of the properties of ice clouds. *Journal of Geophysical Research*, *115*, D00H29. https://doi.org/10.1029/2009JD012346

Dufresne, J. L., & Bony, S. (2008). An assessment of the primary sources of spread of global warming estimates from coupled atmosphere–ocean models. *Journal of Climate*, *21*, 5135–5144.

Hagihara, Y., Okamoto, H., & Yoshida, R. (2010). Development of a combined CloudSat/CALIPSO cloud mask to show global cloud distribution. *Journal of Geophysical Research*, *115*, D00H33. https://doi.org/10.1029/2009JD012344

Harada, Y., Kamahori, H., Kobayashi, C., Endo, H., Kobayashi, S., Ota, Y., … Takahashi, K. (2016). The JRA-55 reanalysis: Representation of atmospheric circulation and climate variability. *Journal of the Meteorological Society of Japan*, *94*, 269–302. https://doi.org/10.2151/jmsj.2016-015

Hogan, R. J., Behera, M. D., O'Connor, E. J., & Illingworth, A. J. (2004). Estimate of the global distribution of stratiform supercooled liquid water clouds using the LITE lidar. *Geophysical Research Letters*, *31*, L05106. https://doi.org/10.1029/2003GL018977

Hoose, C., & Möhler, O. (2012). Heterogeneous ice nucleation on atmospheric aerosols: A review of results from laboratory experiments. *Atmospheric Chemistry and Physics*, *12*, 9817–9854. https://doi.org/10.5194/acp-12-9817-2012

Kanitz, T., Seifert, P., Ansmann, A., Engelmann, R., Althausen, D., Casiccia, C., & Rohwer, E. G. (2011). Contrasting the impact of aerosols at northern and southern midlatitudes on heterogeneous ice formation. *Geophysical Research Letters*, *38*, L17802, 2011. https://doi.org/10.1029/2011GL048532

Kawamoto, K., & Hayasaka, T. (2008). Relative contributions to surface shortwave irradiance over China: A new index of potential radiative forcing. *Geophysical Research Letters*, *35*, L17809. https://doi.org/10.1029/2008GL035083

Kobayashi, T. (1961). The growth of snow crystals at low supersaturations. *Philosophical Magazine*, *6*, 1363–1370.

Kobayashi, S., Ota, Y., Harada, Y., Ebita, A., Moriya, M., Onoda, H., … Takahashi, K. (2015). The JRA-55 reanalysis: General specifications and basic characteristics. *Journal of the Meteorological Society of Japan*, *93*, 5–48. https://doi.org/10.2151/jmsj.2015-001

Korolev, A. (2007). Limitations of the Wegener–Bergeron–Findeisen mechanism in the evolution of mixed-phase clouds. *Journal of the Atmospheric Sciences*, *64*, 3372–3375. https://doi.org/10.1175/JAS4035.1

Korolev, A., & Field, P. R. (2008). The effect of dynamics on mixed-phase clouds: Theoretical considerations. *Journal of the Atmospheric Sciences*, *65*, 66–86. https://doi.org/10.1175/2007JAS2355.1

Ladino Moreno, L. A., Stetzer, O., & Lohmann, U. (2013). Contact freezing: A review of experimental studies. *Atmospheric Chemistry and Physics*, *13*, 9745–9769. https://doi.org/10.5194/acp-13-9745-2013

Liou, K. N. (1986). Influence of cirrus clouds on weather and climate processes: A global perspective. *Monthly Weather Review*, *114*, 1167–1199.

Lohmann, U., & Feichter, J. (2005). Global indirect aerosol effects: A review. *Atmospheric Chemistry and Physics*, *5*, 715–737.

Morrison, H., de Bore, G., Feingold, G., Harrington, J., Shupe, M. D., & Sulia, K. (2012). Resilience of persistent Arctic mixed-phase clouds. *Nature Geoscience*, *5*, 11–17. https://doi.org/10.1038/ngeo1332

Onogi, K., Tsutsui, J., Koide, H., Sakamoto, M., Kobayashi, S., Hatsushika, H., … Taira, R. (2007). The JRA-25 reanalysis. *Journal of the Meteorological Society of Japan*, *85*, 369–432. https://doi.org/10.2151/jmsj.85.369

Okamoto, H., Sato, K., & Hagihara, Y. (2010). Global analysis of ice microphysics from CloudSat and CALIPSO: Incorporation of specular reflection in lidar signals. *Journal of Geophysical Research*, *115*, D22209. https://doi.org/10.1029/2009JD013383

Ou, S.-C., & Liou, K. N. (1995). Ice microphysics and climatic temperature feedback. *Atmospheric Research*, *35*, 127–138.

Partain, P. (2007). Cloudsat ECMWF-AUX auxiliary data process description and interface control document, Cooperative Institute for Research in the Atmosphere. Colorado State University (pp. 11).

Sato, K., & Okamoto, H. (2011). Refinement of global ice microphysics using spaceborne active sensors. *Journal of Geophysical Research*, *116*, D20202. https://doi.org/10.1029/2011JD015885

Seifert, P., Ansmann, A., Mattis, I., Wandinger, U., Tesche, M., Engelmann, R., … Haustein, K. (2010). Saharan dust and heterogeneous ice formation: Eleven years of cloud observations at a central European EARLINET site. *Journal of Geophysical Research*, *115*, D12204. https://doi.org/10.1029/2009JD013222

Stephens, G. L., Vane, D. G., Boain, R. J., Mace, G. G., Sassen, K., Wang, Z., … The CloudSat Science Team. (2002). The CloudSat mission and the A-train. *Bulletin of the American Meteorological Society*, *83*, 1771–1790. https://doi.org/10.1175/BAMS-83-12-1771

Stephens, G. L. (2005). Cloud feedbacks in the climate system: A critical review. *Journal of Climate*, *18*, 237–273.

Takahashi, N., Hayasaka, T., & Okamoto, H. (2016). Differences in ice cloud microphysical properties between western and eastern tropical Pacific regions derived from CloudSat and CALIPSO measurements. *SOLA*, *12*, 91–95. https://doi.org/10.2151/sola.2016-021

Winker, D. M., Hunt, W. H., & McGill, M. J. (2007). Initial performance assessment of CALIOP. *Geophysical Research Letters*, *34*, L19803. https://doi.org/10.1029/2007GL030135

Yoshida, R., Okamoto, H., Hagihara, Y., & Ishimoto, H. (2010). Global analysis of cloud phase and ice crystal orientation from Cloud-Aerosol Lidar and Infrared Pathfinder Satellite Observation (CALIPSO) data using attenuated backscattering and depolarization ratio. *Journal of Geophysical Research*, *115*, D00H32. https://doi.org/10.1029/2009JD012334

Zhang, D., Wang, Z., & Liu, D. (2010). A global view of midlevel liquid-layer topped stratiform cloud distribution and phase partition from CALIPSO and CloudSat measurements. *Journal of Geophysical Research*, *115*, D00H13. https://doi.org/10.1029/2009JD012143

Zhang, D., Wang, Z., Heymsfield, A., Fan, J., Liu, D., & Zhao, M. (2012). Quantifying the impact of dust on heterogeneous ice generation in midlevel supercooled stratiform clouds. *Geophysical Research Letters*, *39*, L18805. https://doi.org/10.1029/2012GL052831

How to cite this article: Yamauchi A, Kawamoto K, Okamoto H. Differences in the fractions of ice clouds between eastern and western parts of Eurasian continent using CALIPSO in January 2007. *Atmos. Sci. Lett*. 2018;19:e807. https://doi.org/10.1002/asl.807